

## Comparison of performance of different working fluids suitable for low temperature jet-refrigeration system

C. Manimaran<sup>\*\*1</sup>, A. Sathiamourthy<sup>2</sup>, A. Selvaraju<sup>3</sup>

<sup>1,3</sup>Department of Mechanical Engineering, Pondicherry Engineering College, Puducherry 605 014, India

<sup>2</sup>Associate Professor, Department of Mechanical Engineering, IFET College of Engineering, Villupuram-605108, India<sup>\*\*</sup>

**Article History:** Received: 11 January 2021; Revised: 12 February 2021; Accepted: 27 March 2021; Published online: 10 May 2021

### Abstract

A refrigeration system, which can be operated using environment-friendly refrigerants, is most welcome nowadays to mitigate environmental issues. In this regard, six refrigerants (R290, RE170, R717, R123, R600a and R601) possessing zero-ODP but GWP less than 100 have been chosen for assessing their performance in vapour jet refrigeration system. A simulation code in FORTRAN77 has been developed to investigate the performance of the refrigeration system along with that of ejector at its choking-mode of operation. The influence of nature of refrigerants as wet and dry fluids on the overall performance has also been investigated. It is understood that the nature of working fluids does not influence much on the performance of the system so as to ascertain that a wet or dry fluid is better than the other in the selected range of operation. The study reveals that the performance of the system with wet or dry refrigerants depends on the thermal and thermodynamic properties, while the physical and chemical properties of refrigerants are predominant in differentiating the performance of dry and wet refrigerants from one another.

**Keywords:** Ejector, Choking, Refrigeration, Environment-friendly refrigerants, Solar energy

### 1. INTRODUCTION

The global energy consumption for cooling applications and air conditioning commercial and residential buildings is found close to 40% of the electricity produced from depleting energy sources predominantly fossil matters available below the Earth's surface [1]. The utilization of electrical energy in larger quantity abets greatly to global warming and greenhouse gas emissions. Since refrigeration along with cooling of space finds a vast application ranging from safeguarding medicines and other health-care consumables to preservation of perishable items like beverage, baked food, meat, poultry, fish, fruits, vegetables, it has become an inevitable part of day-to-day life of people in this modern era. With a view to implement energy security and conserve fossil resources, cooling technologies are being redesigned and tested for their satisfactory performance with renewable and low-grade energy like solar energy to power the technological systems including refrigerating machines. Though vapour compression refrigeration system (VCRS) has made its presence in the field of refrigeration and air-conditioning for more than one century, the requirement of high-grade energy such as electricity for its actuation has made VCRS unsuitable for utilizations of low-temperature sources economically. Owing to the above fact, thermal operated refrigeration systems have become popular and made a revolutionary impact especially in industrial refrigeration and air-conditioning in recent years. A thermal operated refrigeration system can be actuated with solar energy or waste heat from industrial processes. It is always perceived that operation of a thermal operated system is more cost effective when compared with that of work-operated system like VCRS. Vapour absorption, adsorption and vapour jet system technologies are popular among thermal operated refrigeration systems. A vapour absorption refrigeration system fails to realize cooling at generator temperatures less than 80 °C. Further these systems require specialized skills for their construction, operation and maintenance. A vapour adsorption refrigeration system is highly intermittent and restrictive to large scale applications. However, a vapour jet refrigeration system is simple in its operation and maintenance and has very stable performance characteristics. Further, this system can be operated with thermal energy sources at temperatures as low as 60 °C. Heat energy at these temperatures is available from solar flat plate collectors, exhausts from automobiles and waste heat from many industrial processes.

The performance of a vapour jet refrigeration system (VJRS) depends on physical and operational parameters of the ejector, the vital component and the working fluid. Extensive research has been done to understand and improve the performance of VJRS particularly during the second half of the last century [2-8]. The beginning of this century has also witnessed detailed research on VJRS [9-15]. Theories on the basis of fluid dynamics have been proposed for the design of ejector [16-18]. Since jet refrigeration system operating with steam has the drawbacks of very low COP values and being unable to realize temperatures below 0 °C, halocarbon compound refrigerants have found their wide usage for achieving higher values of COP [19-25]. With the total ban on refrigerants in the families of CFCs and HCFCs, which are major contributors to the environmental hazards, much attention is given for halocarbon compound refrigerants that have zero ODP. Many researchers have reported the use of different working fluids in VJRS through their experimental and theoretical investigations. However, optimization of performance of this refrigeration system has become a topic of core interest in order to identify the conditions for the best performance of VJRS. Since a jet refrigeration system involves an ejector as a typical component that emulates the operation a mechanical compressor, the methodology of optimization in VJRS as a whole brings in two different approaches, namely, (i) geometrical optimization that relates to identifying the physical dimensions and features of the ejector, and (ii) thermodynamic optimization that helps to

know the right values of operating parameters like pressure and temperature for maximizing the performance of the system. The former method adopts generally a variable area of ejector by changing the ratio of the area of cross section of mixing tube to the nozzle throat area in an ejector. This paper presents a theoretical analysis of optimal performance of VJRS using variable area method with six different refrigerants (R290, RE170, R717, R123, R600a and R601) that have zero-ODP with GWP less than 20 except R123 which has value of GWP around 77. Among the refrigerants selected for investigation, R290, RE170 and R717 are classified as wet refrigerants while R123, R600a and R601 belongs to dry group. This study probes also the impact of wet and dry refrigerants on the optimal performance of VJRS in the selected range of operating parameters.

## 2. DESCRIPTION OF THE SYSTEM

The schematic diagram of VJRS is shown in Fig. 1. The system consists of a generator, ejector condenser and evaporator. The ejector is the heart of the system. It consists of a convergent-divergent nozzle which is housed in the suction chamber followed by a mixing chamber and diffuser as illustrated in Fig. 2. High pressure primary vapour received from vapour generator passes through the convergent-divergent nozzle. The expansion of primary vapour in convergent-divergent nozzle creates a low pressure at its exit that causes entrainment of secondary vapour from evaporator. When the mixed stream of primary and secondary flow passes through the mixing chamber, it experiences a normal shock that raises the static pressure of the mixed stream. The expansion of primary vapour in convergent-divergent nozzle creates a low pressure at its exit that causes entrainment of secondary vapour from evaporator. The expansion of primary vapour in convergent-divergent nozzle creates a low pressure at its exit that causes entrainment of secondary vapour from evaporator. When the mixed stream of primary and secondary flow passes through the mixing chamber, it experiences a normal shock that raises the static pressure of the mixed stream. A further rise in static pressure occurs in the diffuser. Thus vapour leaves the ejector at a pressure equal to that in the condenser. This vapour is transformed into a saturated liquid in the condenser.

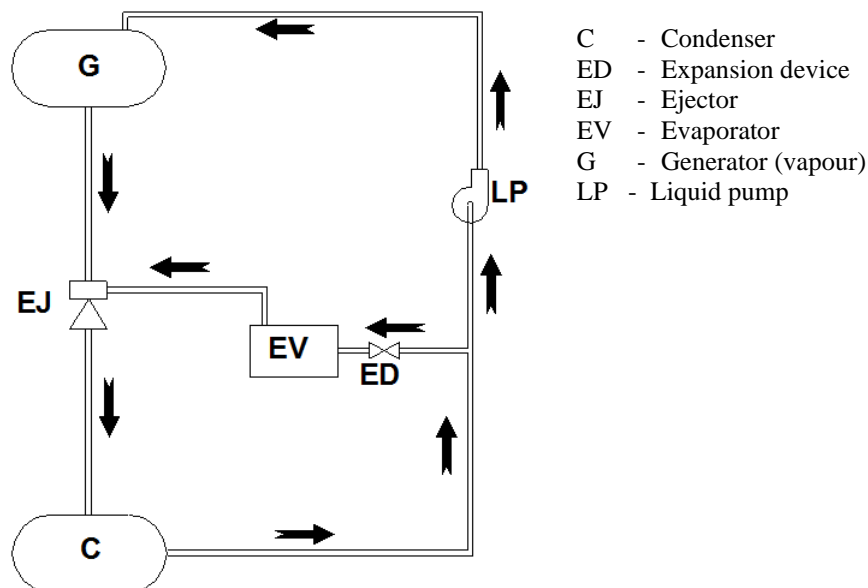


Fig.1 Schematic diagram of VJRS

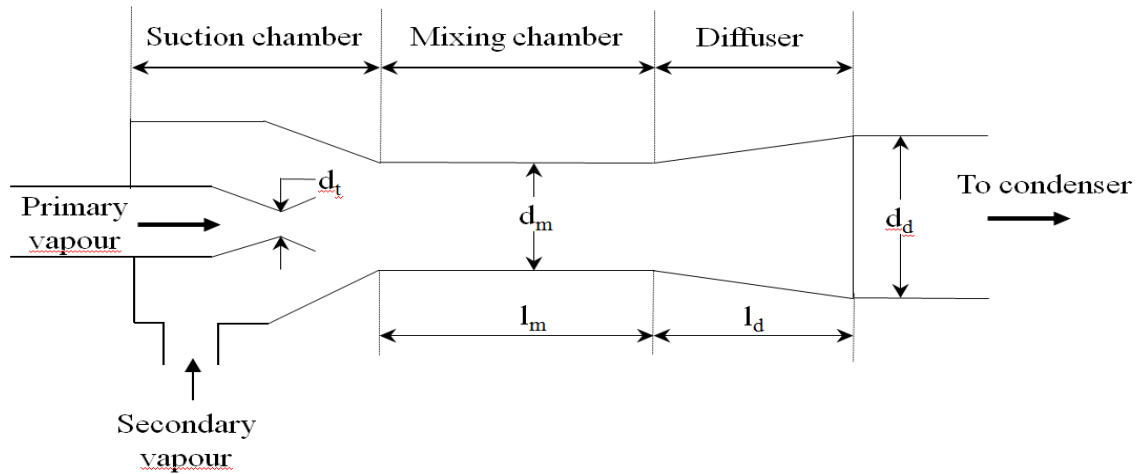


Fig.2 Schematic diagram of ejector

A portion of the liquid refrigerant necessary for realizing refrigeration at the evaporator branches out to the evaporator through expansion device. The remaining portion of the liquid refrigerant is pumped back to the generator through a diaphragm pump. Heat from renewable energy source helps in generation of the primary vapour that actuates the ejector.

### 3. THERMODYNAMIC ANALYSIS

Figure 3 depicts the thermodynamic diagram of vapour jet refrigeration system cycle. The thermodynamic analysis is carried out for a refrigeration system having 0.75 kW of refrigeration capacity.

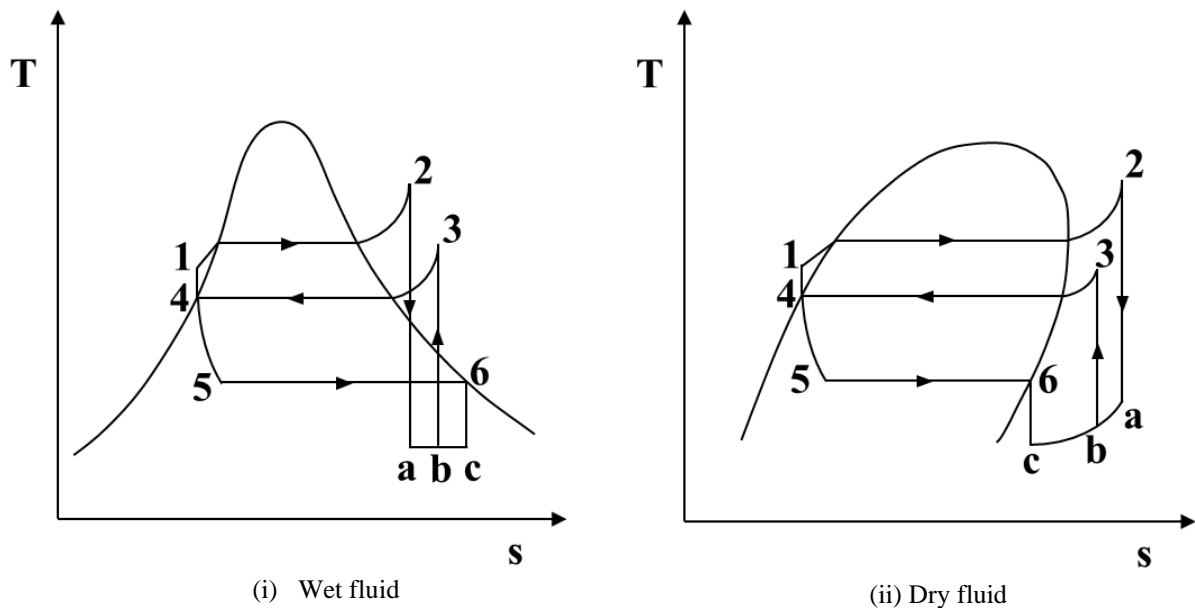


Fig. 3 Thermodynamic cycle of VJRS

#### 3.1 ASSUMPTIONS

The following are assumptions made for the analysis:

- (i) One dimensional flow through the ejector with negligible heat loss
- (ii) Efficiencies of the primary nozzle, the secondary stream passage and the diffuser are 0.95, 0.95 and 0.85 respectively [23]
- (iii) Normal shock occurs within the constant-area mixing chamber

It is learnt from literature [21, 26, 27, 28] that the effect of flow friction in the mixing chamber is more sensitive on ejector performance than factors. Since the mixed vapour enters the mixing chamber at supersonic velocity with high Reynolds number, the friction factor is expressed as [27, 28],

$$\frac{1}{\sqrt{f_m}} = 2.0 \log(\text{Re}_m \sqrt{f_m}) - 0.8 \tag{1}$$

The velocity at the throat of primary nozzle is evaluated as

$$V_t = \sqrt{2\eta_p (h_g - h_t)_{is}} \tag{2}$$

The ratio of area of the throat to mass flow rate is computed as,

$$\frac{A_t}{m_p} = \frac{v_p}{V_t} \tag{3}$$

Velocity of primary vapour leaving the nozzle is

$$V_{pe} = \sqrt{2\eta_p (h_g - h_{pe})_{is}} \tag{4}$$

Velocity of the secondary vapour just before meeting primary fluid is expressed as,

$$V_{se} = \sqrt{2\eta_s (h_e - h_{se})_{is}} \tag{5}$$

The hypothetical area for unit mass flow rate of secondary vapour at given inlet pressure and temperature is found as,

$$\frac{A}{m_s} = \frac{v_s}{V_{se}} \tag{6}$$

The mass flow rate of vapour in the mixing chamber is expressed as,

$$m_m = m_p + m_s \tag{7}$$

Neglecting the body force and internal drag force, the momentum balance across a differential element of thickness  $dx$  and flow area,  $A$  can be obtained by equating change of momentum, net pressure force in the axial direction and wall friction force. Thus, for the horizontal mixing chamber, the differential equation for momentum balance is obtained as,

$$A dp + m dV + \delta F_i = 0 \tag{8}$$

For the cylindrical mixing chamber, the wall friction force is expressed as,

$$\delta F_i = \frac{\rho V^2}{2} \left( \frac{f_m dx}{d_h} \right) A_m \tag{9}$$

where  $d_h$  is the hydraulic diameter and it is equal to  $d_m$ .

In the ejector both primary and secondary vapours enter the mixing chamber and leave it as mixed vapour. Hence, momentum balance between inlet section and section before shock in the mixing chamber can be obtained using Eq. (7) and (8) as,

$$m_p V_{pe} + m_s V_{se} + P_{se} A_m = m_m V_m + P_m A_m + m_m V_m \left( \frac{f_m}{2} \frac{l_m}{d_m} \right) \tag{10}$$

Using Eq. (10), the velocity of the mixed vapour stream is obtained as,

$$V_m = \frac{(m_p V_{pe} + m_s V_{se}) + (P_{se} - P_m) A_m}{m_m \left( 1 + \frac{f_m}{2} \frac{l_m}{d_m} \right)} \tag{11}$$

By mass balance, area of the constant area mixing chamber for unit mass flow rate of mixed vapour flow is rewritten as,

$$\frac{A_m}{m_m} = \frac{v_m}{V_m} \tag{12}$$

The characteristic area ratio for the ejector is obtained with the help of the following expression as,

$$\phi = \frac{A_m}{A_t} = (1 + \mu) \frac{v_m V_t}{v_p V_m} \tag{13}$$

The normal shock is assumed to occur at the mixing chamber. Using mass, momentum and energy balances, the static pressure rise across the shock is given as,

$$P_{as} - P_m = \frac{V_m}{v_m} (V_m - V_{as}) \tag{14}$$

Assuming that the pressure after the shock and the pressure at the diffuser inlet are equal and the mixed stream leaves the diffuser at negligible velocity, the velocity of the fluid at diffuser inlet is determined as,

$$V_{d1} = \sqrt{\frac{2(h_{d2} - h_{d1})_{is}}{\eta_d}} \tag{15}$$

The expression for maximum entrainment ratio is obtained from momentum balance between inlet and exit sections of the mixing chamber as [27, 28],

$$\mu = \frac{V_{pe} - V_{d1} - \frac{1}{2}V_{d1}f_m\left(\frac{l_m}{d_m}\right)}{V_{d1} - V_{se} + \frac{1}{2}V_{d1}f_m\left(\frac{l_m}{d_m}\right)} \quad (16)$$

Generally, the work imparted to the pump is neglected when compared with the heat input to the generator. Hence the COP of the VJR system is expressed as,

$$COP = \mu \frac{(h_e - h_c)}{(h_g - h_c)} \quad (17)$$

### 3.2 COMPUTATIONAL METHODOLOGY

A simulation model has been developed in FORTRAN 77 language on the basis of the one dimensional ejector theory and control-volume-based analytical equations.

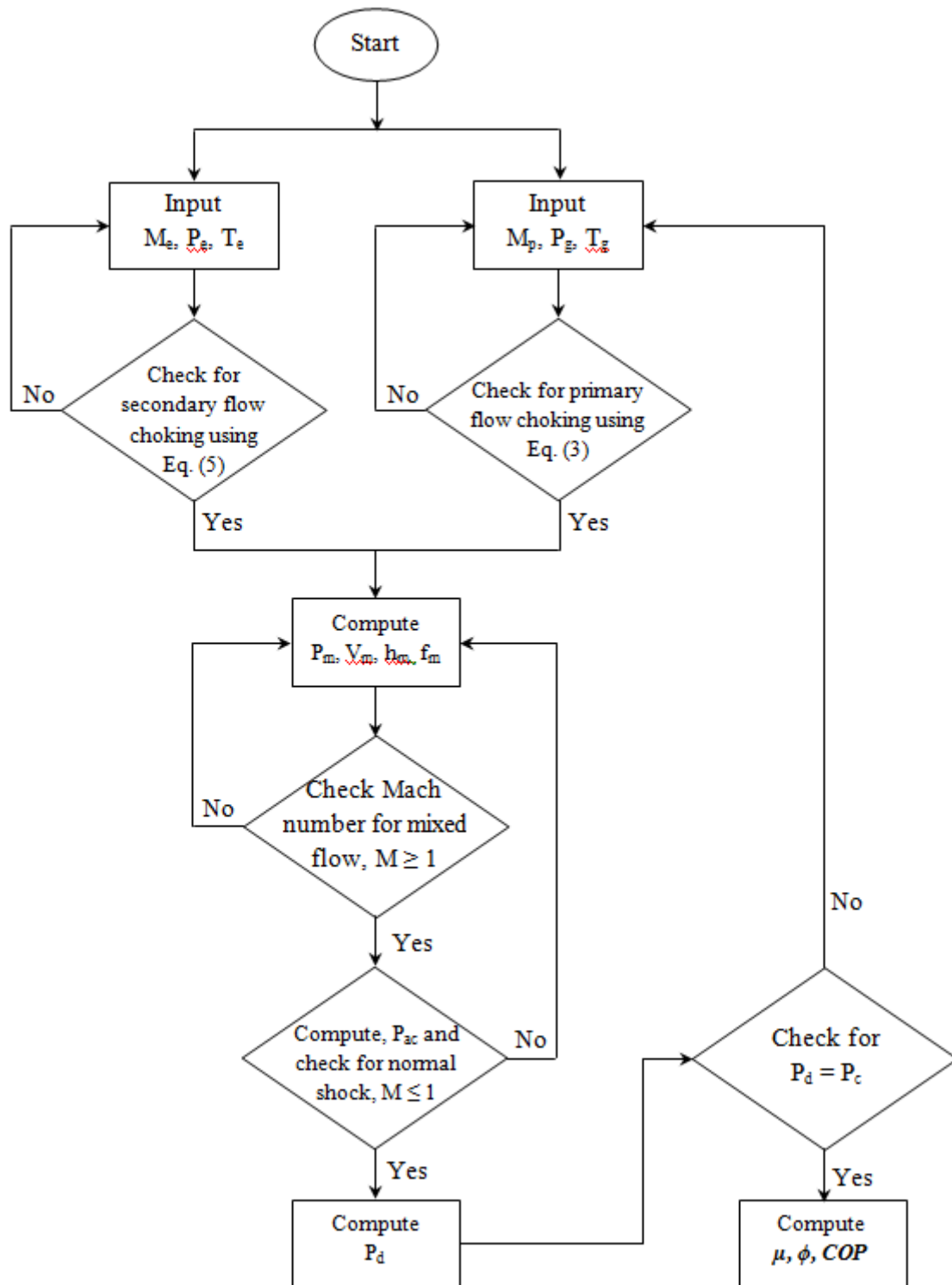


Figure 4 Flow chart depicting simulation methodology

Thermal and thermodynamic properties of working fluids are obtained from literature [29, 30]. The operating parameters, namely,  $T_g$ ,  $T_e$ ,  $T_c$ ,  $P_g$ ,  $P_e$  and  $P_c$  along with mass flow rates of primary and secondary streams have been chosen as inputs for solving the governing equations. The ratio of cylindrical chamber length to diameter is assumed to be 10 [21]. Choking of primary stream as well as secondary vapour at the respective passage has been found out with the ratio of area of the critical sections such as throat to mass flow rate in accordance with Eqs. (3) and (6). The state of the mixed fluid is checked for supersonic flow condition and subsequently the existence of a normal shock at the constant-area mixing chamber is probed if the flow before the shock is supersonic. Neglecting the velocity at the diffuser exit, the total pressure raise across the shock and diffuser is matched for the exit pressure of the diffuser,  $P_c$  by an iterative process wherein the entrainment of secondary fluid is varied and checked for satisfactory results. The procedure followed for analysis is shown in the flow

chart, Figure 4. This computational procedure yields the output of maximum entrainment ratio,  $\mu$ , characteristic area ratio,  $\phi$  and maximum COP.

#### 4. RESULTS AND DISCUSSION

##### 4.1 VALIDATION OF SIMULATION CODE

Validation of the simulation model has been carried with R141b as refrigerant. The influence of generator temperature on characteristic area ratio of ejector has been investigated at  $T_c = 305$  K and  $T_c = 281$  K and the simulated performance is compared with that of experimental data available in the literature [23] as shown in Figure 5. It is observed that this simulated performance results are fairly in good agreement with experimental data with a deviation ranging from  $-5.8\%$  to  $+4.2\%$ .

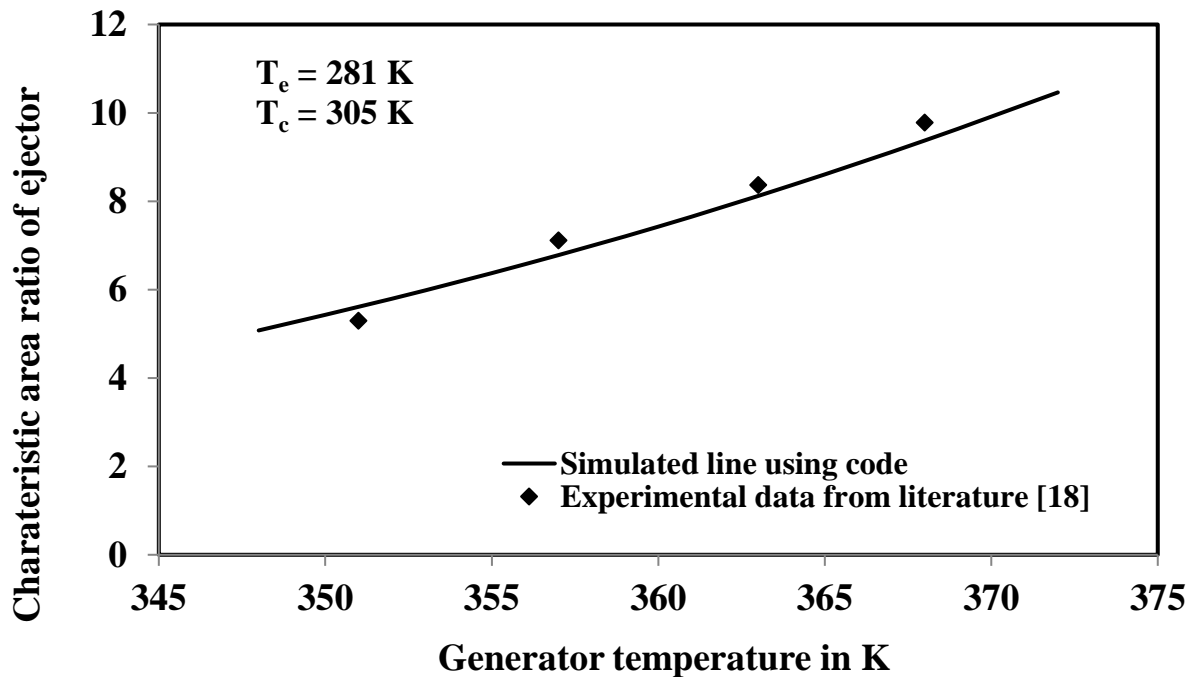


Figure 5 Effect of generator temperature on characteristic area ratio with R141<sub>b</sub>

##### 4.2 VARIATION OF MAXIMUM ENTRAINMENT RATIO

Figure 6 shows the effect of generator temperature on maximum entrainment ratio for the selected six refrigerants. When both condenser and evaporator temperatures remain constant, an increase in generator temperature causes an increase in velocity of driving vapour which is related to the difference in enthalpy between inlet and exit sections in accordance with Eq. (4). This higher velocity of primary stream entrains more secondary stream resulting in an increase in entrainment ratio. In fact, when the ejector operates at its critical mode the maximum entrainment ratio increases with the increase in generator temperature. The back pressure at the ejector exit goes up. Any increase in the back pressure at the given generator and evaporator temperatures reduces the rate of entrainment due to increase in compression ratio. Hence critical entrainment ratio decreases as the condenser temperature increases. The performance of R290 is found better among the wet group while that of R123 is comparatively higher. The lowest performance is observed with R717 among wet refrigerants and R601 among dry refrigerants.

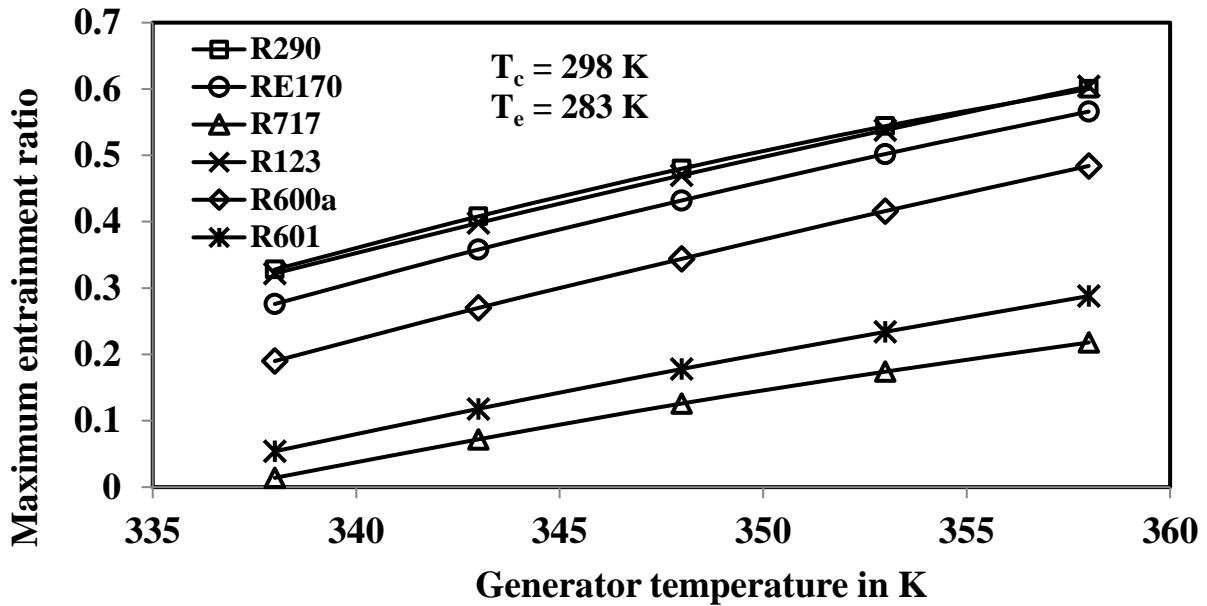


Figure 6 Variation of maximum entrainment ratio with generator temperature

It is observed that the maximum entrainment ratio increases with increase in evaporator temperature as illustrated in Figure 7. The increase in evaporator temperature results into an increase in enthalpy of secondary stream at its entry to the ejector system. This higher enthalpy at the entry section leads to a rise in the velocity of secondary stream in line with Eq. (5), which results in induction of more secondary vapour into the mixing chamber. The better as well as poorer performance among the selected refrigerants is found to show similar trends as that of generator temperature presented earlier.

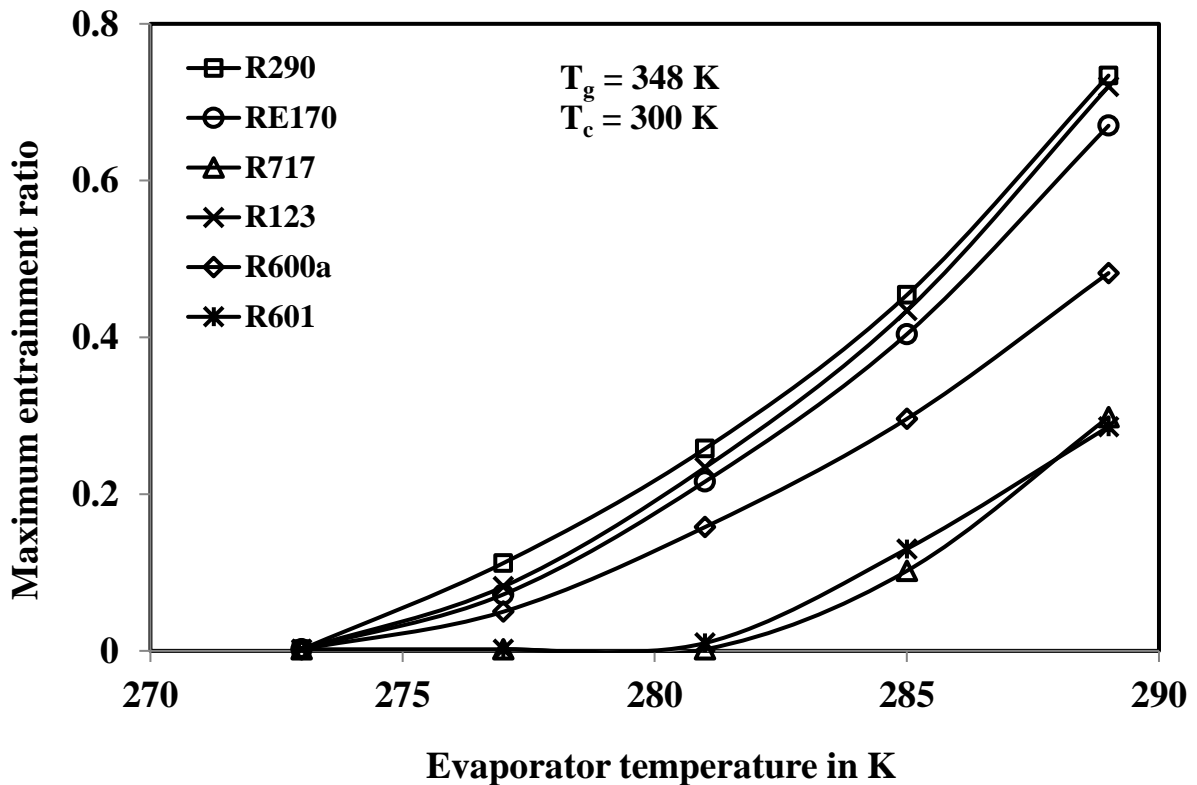


Figure 7 Variation of maximum entrainment ratio with evaporator temperature

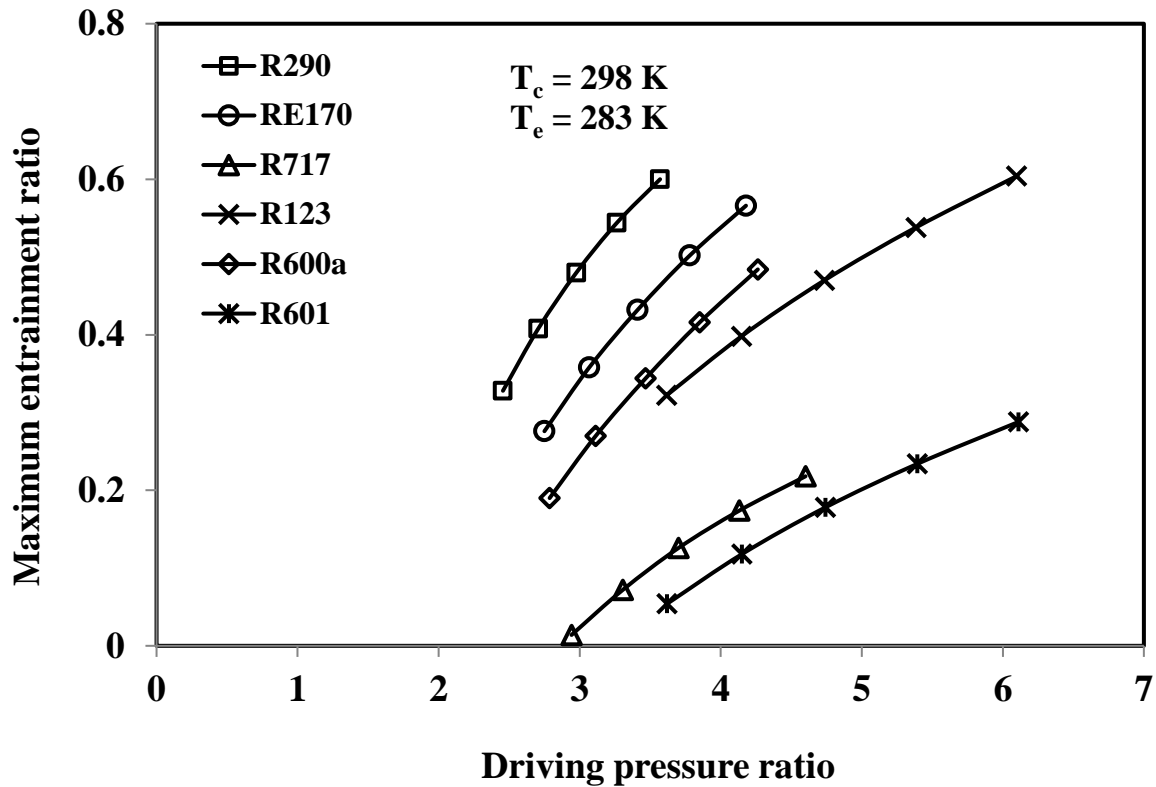


Figure 8 Variation of maximum entrainment ratio with driving pressure ratio

The effect of driving pressure ratio on maximum entrainment ratio is shown in Figure 8. The driving pressure ratio is always related to  $P_g$  and hence an increase in driving pressure ratio at the given condenser pressure makes the maximum entrainment ratio increase due to increased momentum of primary stream. The selected refrigerants show similar order of merits of performance in comparison with that of generator temperature and evaporator temperature.

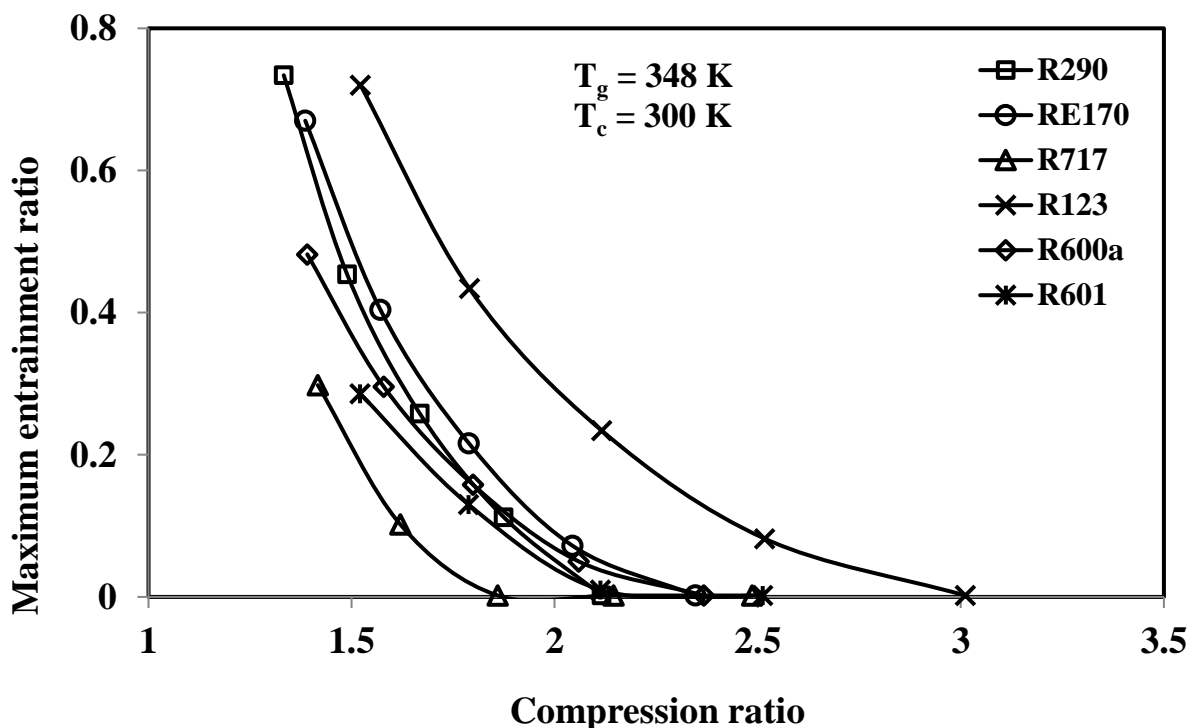


Figure 9 Variation of maximum entrainment ratio with compression ratio

The compression ratio ( $P_c/P_e$ ) is directly related to the ratio of respective temperatures. This implies that an increase in compression ratio necessitates more primary vapour mass flow to entrain the same secondary vapour flow at the given condenser and generator temperatures. This higher quantity of primary streams leads to reduction in maximum entrainment ratio as shown in Figure 9. It is noted that this decrease in maximum entrainment ratio with the increase in compression ratio is common for all six working fluids but at different ranges of values. It is observed further that the influence of compression ratio on maximum entrainment ratio becomes insignificant for two working fluids, namely, R717 and R601. Because the induction of secondary vapour is found to be negligible at higher compression ratio which in turn makes the value of maximum entrainment ratio approaching to zero in the selected range of operating conditions. It is further observed that R290 (wet refrigerant) and R123 (dry refrigerant) perform better in their respective range of compression ratio.

#### 4.2 VARIATION OF MAXIMUM COP

It is understood from Figure 6 that the maximum entrainment ratio increases with increase in generator temperature while the condenser and evaporator temperatures remain constant. It can be further noted that the increase in enthalpy difference ( $h_g - h_c$ ) dictates a reduction in primary vapour flow rate to entrain the same secondary vapour flow. But the reduction in the primary vapour flow rate overrides the increase in enthalpy difference ( $h_g - h_c$ ). Also, COP is directly proportional to entrainment ratio. Hence the critical COP increases when the generator temperature increases as shown in Figure 10. The rank of performance of wet and dry refrigerants is found similar to that of maximum entrainment ratio illustrated in Figure 6.

Figure 11 portrays the variation of maximum COP with evaporator temperature at the given generator and condenser temperatures. The refrigerating effect ( $h_e - h_c$ ) increases when the evaporator temperature increases for the given condenser temperature while the denominator in Eq. 17 remains the same. Hence the maximum COP increases when the evaporator temperature increases. The better and poor performances of wet and dry refrigerants are found similar to that of maximum entrainment ratio illustrated in Figure 7.

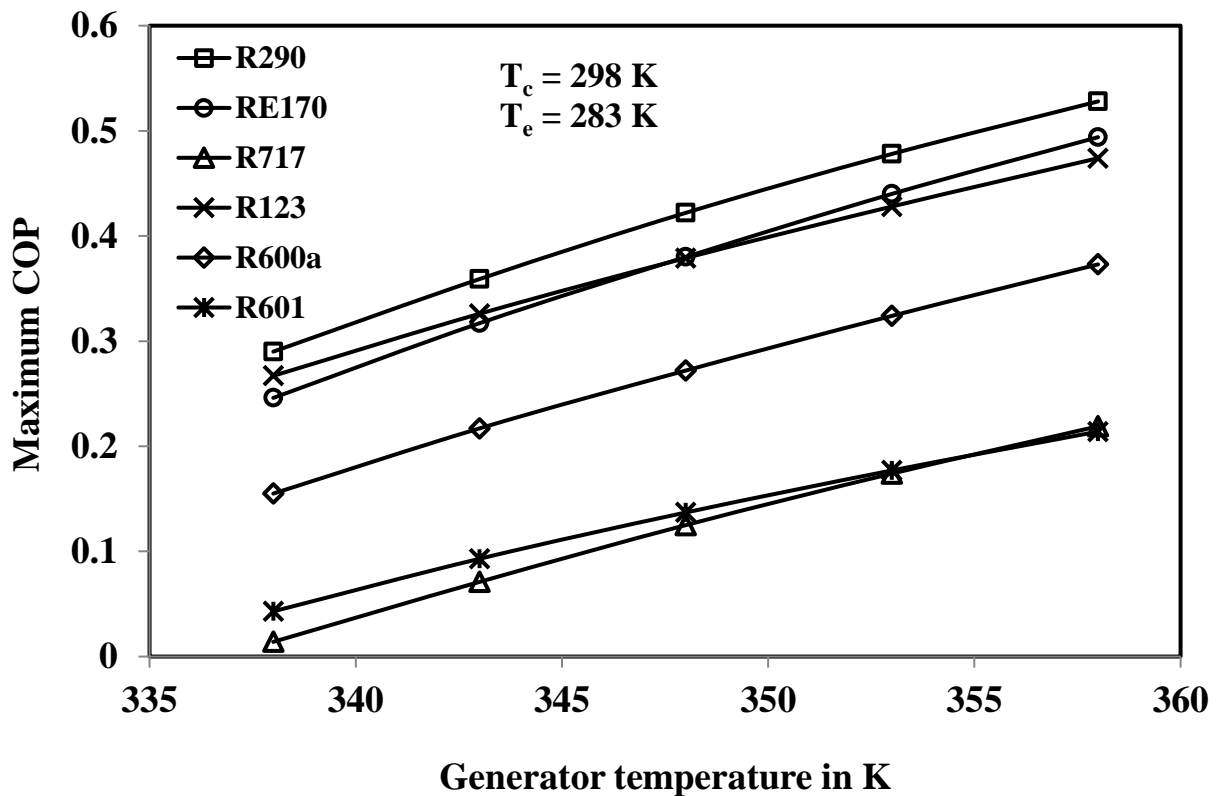


Figure 10 Effect of generator temperature on maximum COP

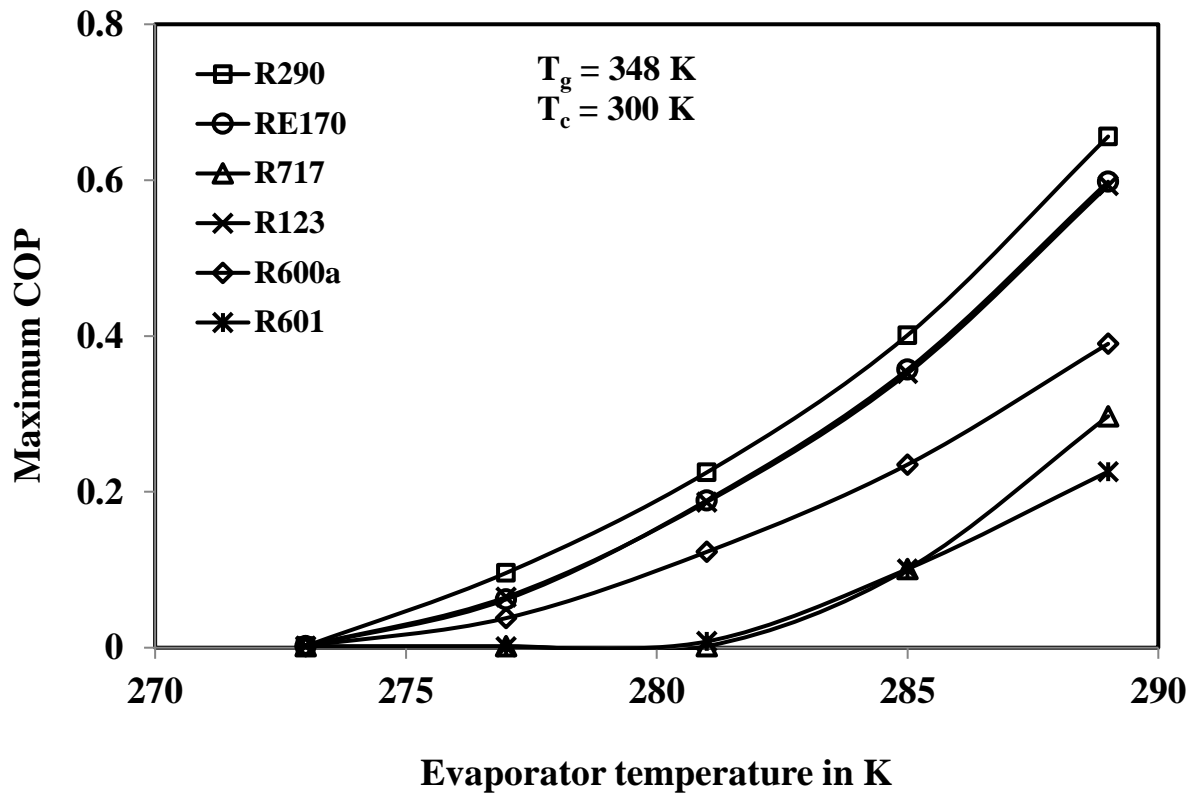


Figure 11 Effect of evaporator temperature on maximum COP

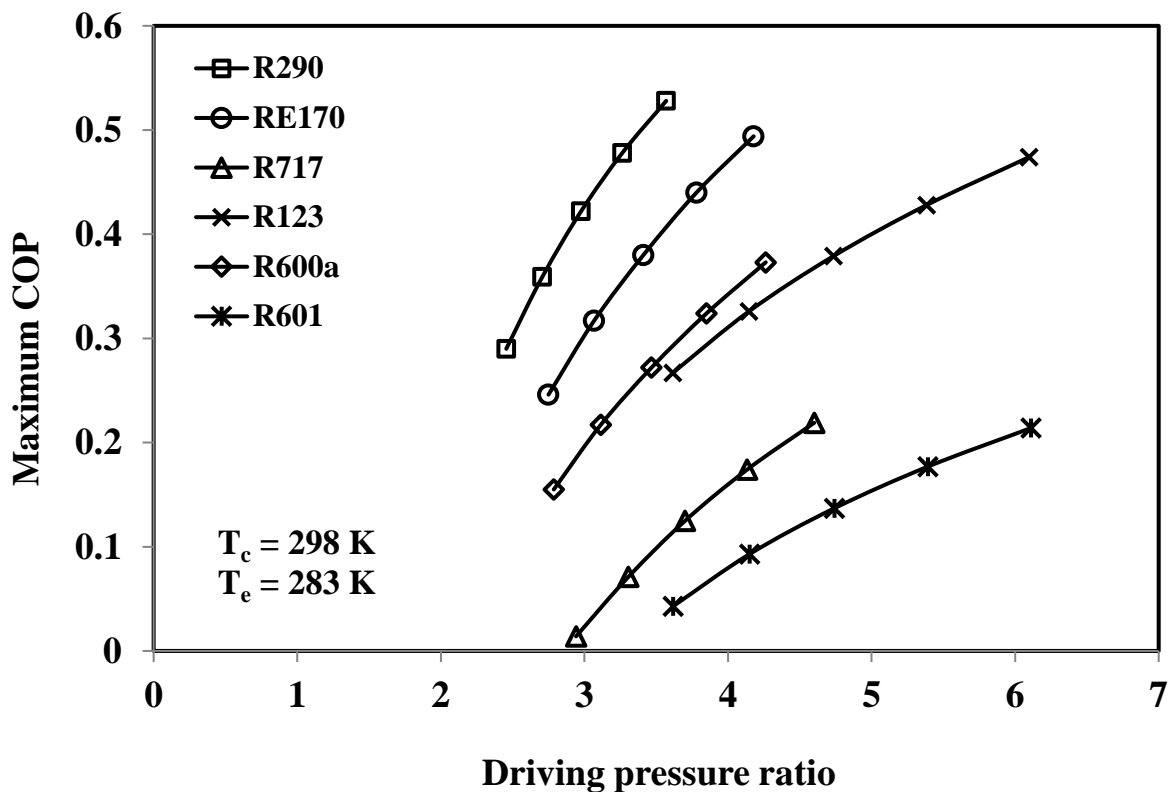


Figure 12 Effect of driving pressure ratio on maximum COP

Figure 12 discerns the variation of maximum COP with driving pressure ratio. It is noted from Figure 7 that when the driving pressure ratio increases at the given condenser temperature the back pressure at the ejector exit decreases. This helps to induct more secondary vapour from the evaporator. The rate of removal of more quantity of secondary vapour causes an increase in refrigerating effect and a simultaneous increase in maximum COP. R290 and R123 exhibit better performance among wet and dry groups respectively.

When the compression ratio increases at the given evaporator temperature the back pressure at the ejector exit increases. This retards the induction of secondary vapour into the ejector and consequently reduces the entrainment ratio. A lower entrainment ratio indicates in turn a drop in COP. Thus the maximum COP decreases when compression ratio increases as shown in Figure 12 for all selected refrigerants.

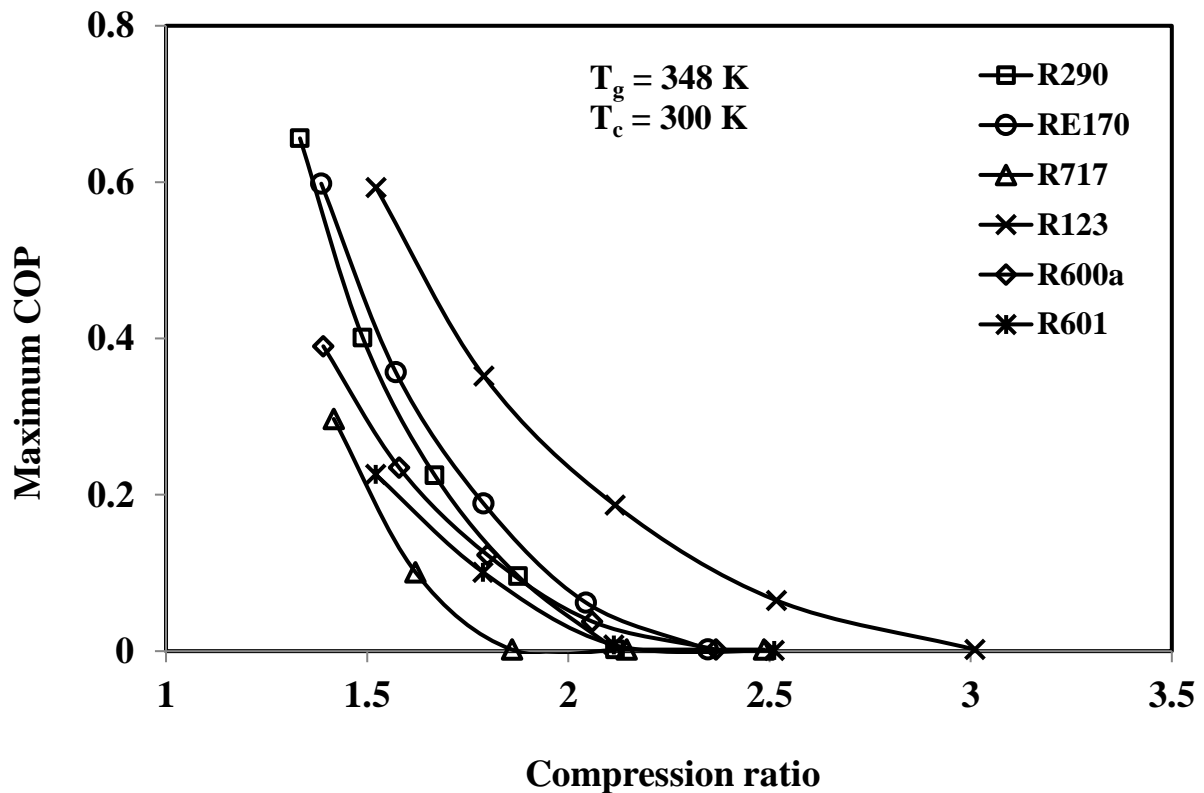


Figure 13 Effect of compression ratio on maximum COP

### 5. CONCLUSIONS

The maximum entrainment ratio and maximum COP of R290 and R123 are found higher in comparison with other refrigerants in wet and dry fluids respectively. It is difficult to assess from the level of performance of each refrigerant that a wet refrigerant performs always better than a dry refrigerant or vice versa. However, it is inferred that the disparity in performance of the selected refrigerants is attributed to the momentum of primary vapour issuing from the nozzle along with that of secondary vapour before mixing and the viscous force experienced by each stream of respective refrigerant at the hypothetical shear layer formed between primary and secondary stream [27]. Further, the performance of the system with wet or dry refrigerants depends on the thermal and thermodynamic properties, while the physical and chemical properties of refrigerants are predominant in differentiating the performance of dry and wet refrigerants from one another.

#### Nomenclature

<i>A</i>	area (m <sup>2</sup> )
<i>d</i>	diameter (m)
<i>f</i>	friction factor
<i>h</i>	specific enthalpy (kJkg <sup>-1</sup> K <sup>-1</sup> )
<i>l</i>	length (m)
<i>m</i>	mass flow rate (kg s <sup>-1</sup> )
<i>P</i>	pressure (kPa)
<i>T</i>	temperature (K)
<i>v</i>	specific volume (m <sup>3</sup> kg <sup>-1</sup> )
<i>V</i>	velocity (m s <sup>-1</sup> )

#### Greek

$\phi$	characteristic area ratio of ejector, $\phi = A_m/A_t$
$\eta$	efficiency
$\mu$	maximum entrainment ratio, $\mu = m_s/m_p$

#### Subscripts

<i>c</i>	condenser
<i>d</i>	diffuser

---

$d_1$	diffuser inlet
$d_2$	diffuser outlet
$e$	evaporator
$g$	generator
$is$	isentropic
$m$	mixing chamber
$p$	primary fluid
$pe$	primary fluid exit
$t$	throat
$s$	secondary fluid
$se$	secondary fluid exit

**Abbreviation**

CFC	chlorofluorocarbon
COP	coefficient of performance
GWP	Global warming potential
HCFC	hydrochlorofluorocarbon
ODP	Ozone depletion potential
VCRS	vapour compression refrigeration system
VJRS	vapour jet refrigeration system

**REFERENCES**

- [1] N. Y. Jadhav, Green and Smart Building - Advanced Technology Options, Springer, Singapore, 2016
- [2] L.A. Defrate, and A.E. Hoerl, Optimum design of ejector using digital computers, Chemical Engineering Progress Symposium Series 55 (21) (1959) 43-51
- [3] F. Zeren, R.E Holmes, P.E. Jenkins, Design of a freon jet pump for use in a solar cooling system, ASME Winter Annual Meeting, (1978) 1- 9.
- [4] R. Dorantes, A. Lallemand, Prediction of performance of a jet cooling system operating with pure refrigerants or non-azeotropic mixtures, Int. J. Refrig. 18(1) (1995) 21–30
- [5] Sokolov, M. and Hershgal, D., (1990), 'Enhanced ejector refrigeration cycles powered by low grade heat - Part 1: System characterisation', Int. J. Refri., 13, 351-356.
- [6] Sokolov, M. and Hershgal, D., (1990), 'Enhanced ejector refrigeration cycles powered by low grade heat - Part 2: Design procedures', Int. J. Refri., 13, 357-363.
- [7] Sokolov, M. and Hershgal, D., (1990), 'Enhanced ejector refrigeration cycles powered by low grade heat - Part 3: Experimental results', Int. J. Refri., 14, 24 -31.
- [8] L. Boumaraf, A. Lallemand, Performance of a jet cooling system using refrigerants mixtures, Int. J. Refrig. 22 (1999) 580 – 589
- [9] T. Sankarlal, and A. Mani (2006) Experimental studies on an ammonia ejector refrigeration system, Int. Commn. Heat and Mass Transfer, 33, 224–230
- [10] Chen, J., Havtun, H., Palm, B. (2014) Screening of working fluids for the ejector refrigeration system, International Journal of Refrigeration, 47, pp. 1-14
- [11] Hamzaoui, M., Nesreddine, H., Aidoun, Z., Balistrrou, M. (2018) Experimental study of a low grade heat driven ejector cooling system using the working fluid R245fa. International Journal of Refrigeration, 86, 388–400
- [12] Besagni, G. (2019) Ejectors on the cutting edge: The past, the present and the perspective. Energy, 170, 998–1003
- [13] Besagni, G., Mereu, R., Inzoli, F. (2016) Ejector refrigeration: A comprehensive review. Renew. Sustain. Energy Rev., 53, 373–4
- [14] Shovon, M. K. B., Senthil Kumar, R., Suryan, A., Kim, T H., Kim, H. D., 2020. Performance of ejector refrigeration cycle based on solar energy working with various refrigerants, J. Thermal Analysis and Calorimetry. 141, 301–312.
- [15] Saleh, B., 2016. Performance analysis and working fluid selection for ejector refrigeration cycle, Applied Thermal Engineering. 107, 114–124
- [16] J.H. Keenan, E.P. Neumann, F. Lustwerk , An investigation of ejector design by analysis and experiment, ASME Annual meeting, (1949) 299- 309.
- [17] J.T. Munday, and D.F. Bagster, A new theory applied to steam jet refrigeration, Ind. Eng. Chem. Process Des. Dev., 16 (4) (1977) 442-449
- [18] Dutton, J.C. and Carroll, B.F., (1986), 'Optimal supersonic ejector design', ASME J. Fluids Engg., Vol. 108, 414-420.
- [19] E. Nahdi, J.C. Champoussin, G. Hostache, J. Cheron, Optimal geometric parameters of a cooling ejector-compressor, Int. J. Refrig. 16(1) (1993) 67 -72
- [20] S. Srinivasa Murthy, R. Balasubmanian and M.V. Krishna Murthy (1991) Experiments on vapour jet refrigeration system suitable for solar energy applications, Renewable Energy, 1, 757-768

- [21] P.Paliwoda, A review paper on the experimental study on low-grade heat and solar energy operated halocarbon vapour-jet refrigeration systems, Topical studies, IIR Bull. (1968) 1003
- [23] B.J. Huang, J.M. Chang, C.P. Wang, V.A. Petrenko, A 1-D analysis of ejector performance, Int. J. Refrig., 22 (1999) 354 -364.
- [24] B.J. Huang, J.M. Chang, Empirical correlation for ejector design, Int. J. Refrig., 22 , (1999) 379 - 388.
- [25] J.J. Henzler, Design of ejectors for single-phase material systems, Ger. Chem. Eng., 6(1983) 292
- [26] K. Cizungu, A. Mani, M. Groll, Performance comparison of vapour jet refrigeration system with environmentally friendly working fluids, Applied Thermal Engineering, 21 (2001) 585-595.
- [27] A. Selvaraju, Mani A., Analysis of an ejector with environment friendly refrigerants, Applied Thermal Engineering, 2004;21;585-95.
- [28] A. Selvaraju, Mani A., Analysis of a vapour ejector refrigeration system with environment friendly refrigerants, Int J Thermal Sciences, In print.
- [29] C. Borgnakke and R.E. Sonntag, Thermodynamic and transport properties, John Wiley & Sons. Inc, 1997
- [30] ASHRAE Handbook-Fundamentals: Chapter 30 Thermophysical Properties of Refrigerants, American Society of Heating, Air Conditioning and Refrigeration Engineers, Atlanta, GA, 2013